Fermi surface topology and nontrivial Berry phase in the flat-band semimetal Pd_3Pb

Mojammel A. Khan,[1,*] Po-Hao Chang,[2] Nirmal Ghimire,[1,†] Terence M. Bretz-Sullivan,[1] Anand Bhattacharya,[1] J. S. Jiang,[1] John Singleton,[3] and J. F. Mitchell[1]

[1]*Materials Science Division, Argonne National Laboratory, 9700 South Cass Avenue, Argonne, Illinois 60439, USA*
[2]*Department of Computational and Data Sciences, George Mason University, 4400 University Dr., Fairfax, Virginia 22030, USA*
[3]*National High Magnetic Field Laboratory, Los Alamos National Laboratory, MS-E536, Los Alamos, New Mexico 87545, USA*

(Received 6 January 2020; revised manuscript received 2 April 2020; accepted 18 May 2020; published 2 June 2020)

A study of the Fermi surface of the putative topological semimetal Pd_3Pb has been carried out using Shubnikov–de Haas (SdH) oscillations measured in fields of up to 60 T. Pd_3Pb has garnered attention in the community due to a peculiar Fermi surface that has been proposed theoretically by Ahn, Pickett, and Lee, Phys. Rev. B **98**, 035130 (2018) to host a dispersionless band along $X - \Gamma$ as well as multiple triply degenerate band crossings that, under the influence of spin-orbit coupling, lead to ten fourfold degenerate Dirac points. Analysis of the SdH oscillation data verifies the calculated multisheet Fermi surface, revealing a Γ centered spheroid that had not been resolved experimentally in prior studies. A comprehensive, angle-dependent analysis of the phase of the SdH oscillations convincingly demonstrates a nontrivial Berry phase for two bands along $\Gamma - R$, supporting the theoretical predictions, while simultaneously evidencing interference between extremal orbits that mimics a trivial Berry phase at intermediate angles.

DOI: 10.1103/PhysRevB.101.245113

I. INTRODUCTION

Crystalline solids have emerged as novel testbeds in the search for exotic fundamental particles [1,2]; for example, three-dimensional topological semimetals offer a chance to explore new topological phases beyond those predicted in high-energy physics [3–5]. Along this journey, many new phases have been discovered, including skyrmions [6], Weyl fermions [7], and Majorana fermions [8]. These discoveries not only access the fundamental physics of unusual particles, but also suggest the application of such exotic states to future technologies such as spin-based electronics and quantum computation.

Recently, the cubic compound, Pd_3Pb, has been proposed [9] to host a novel triple point (TP) fermionic phase with threefold degeneracies along certain high symmetry lines. In addition to the triple points, Pd_3Pb also exhibits a dispersionless band along the $\Gamma - X$ line that lies close to the Fermi energy (E_F). Band-structure calculations in the absence of spin-orbit coupling (SOC) show a combination of triple nodal points and three-dimensional nodal rings, giving rise to topological surface states along the $\Gamma - R$ and $R - M$ lines. The inclusion of SOC produces ten fourfold-degenerate Dirac points as well as topological character on the $k_z = 0$ plane.

Recent transport studies of Pd_3Pb have revealed a large nonsaturating magnetoresistance and a high mobility, $\mu \approx 2 \times 10^3$ cm^2 V^{-1} s^{-1} [10]. In another study, torque magnetometry has been utilized to explore the Fermi surface (FS), which shows the existence of several electron and hole pockets with small carrier masses [11]. However, a complete picture of the FS topology including the topological aspects of the bands, is yet to be reported. Moreover, the crystals used in torque studies were found to be doped to an equivalent of 3% Bi-substitution on the Pb site, placing $E_F \approx 50$ meV above that calculated by density functional theory (DFT) [11]. It was asserted that ≈1% Bi-doping is required to place E_F precisely on the flat band [9]. In this study, we use quantum oscillations measured on oriented single crystals of Pd_3Pb to complete an experimental mapping of the FS, revealing a previously unresolved hole pocket at Γ. From the frequency dependence on the position of E_F, we find our crystals to be slightly electron doped, placing the $E_F \approx 30$ meV above the calculated value of E_F for nominal Pd_3Pb. Importantly, we show that the bands between $\Gamma - R$ and $R - M$ give rise to nontrivial Berry phase, validating the topological features identified by theory [9].

Single crystals of Pd_3Pb were grown using a self-flux method described elsewhere [10]. Shubnikov–de Haas (SdH) oscillations were measured in both low field [up to 14 T in a Quantum Design Physical Property Measurement System (PPMS)] and at high field in a 65 T magnet at the National High Magnetic Field Laboratory (NHMFL) Pulsed-Field Facility [12]. A detailed description of experimental methods are provided in the Supplemental Material (SM) [13].

II. RESULTS AND DISCUSSIONS

Figure 1(a) shows the SdH oscillations measured through a change in resonant frequency, Δf, and hence the magnetoresistance (MR), since $\Delta f \propto -\Delta\rho$ [14]. The increasing MR is consistent with previous reports [10]. Upon

*mkhan19@anl.gov
†Present address: Department of Physics and Astronomy, George Mason University, 4400 University Drive, Fairfax, Virginia 22030, USA.

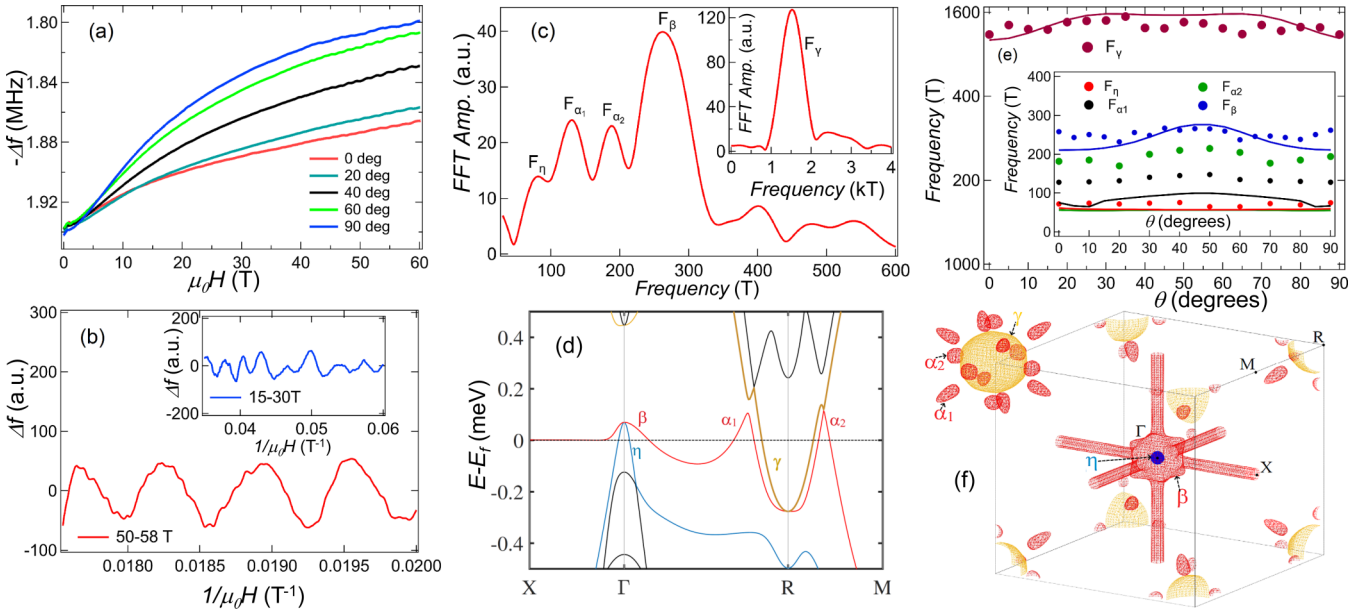

FIG. 1. Shubnikov–de Haas oscillations and Fermi surface of Pd_3Pb. (a) Raw oscillations shown as negative of change in resonant frequency of PDO coil. (b) PDO data shown in two field ranges after a smooth background subtraction: low field, 15–30 T (inset) and high field range, 50–58 T. (c) Fast Fourier transform (FFT) of the oscillation data in two different field ranges. The low and high frequencies are evident. Inset: FFT showing the 1570 T frequency. (d) DFT band structure of Pd_3Pb with spin-orbit coupling expanded over a small energy range to show the electron and hole pockets that are present in the FFTs. (e) Angular dependence of the frequencies identified by FFTs. The solid lines are the theoretical values as described in the text. (f) Fermi surface of nominal Pd_3Pb projected into the first Brillouin zone. The color of the bands are the same as for panel (d). Description of the band structure calculations can be found in the SM [13].

subtraction of a smooth background, the oscillations become more pronounced, as shown in Fig. 1(b), where the field is applied along the a axis. Here the data were divided into two field regimes. The high frequency oscillations are apparent above 50 T. In the field range from 10 to 30 T, a fast Fourier transform (FFT) reveals several low frequencies with broad maxima. This is a consequence of weaker low frequency oscillations in the high field data. The maximum of the FFT peak was also verified via PPMS measurements (see SM [13] Fig. S1). The results of the FFT are shown in Fig. 1(c) with frequencies $F_{\alpha_1} = 128$ T, $F_{\alpha_2} = 182$ T, and $F_\beta = 258$ T, while the high frequency oscillations yield $F_\gamma = 1570$ T. The observed frequencies are in good agreement with previous reports [10,11]. However, we are also able to discern an additional frequency η with $F_\eta = 72$ T, that was not reported in Ref. [11]. The absence of the additional frequency in the torque data can be understood either from the spherical shape of the corresponding FS sheet or the dependence of F_η on the position of E_F (see the SM [13] for further discussion).

The observed frequencies can be related to the calculated band structure shown in Fig. 1(d) for nominal Pd_3Pb. Three hole pockets, η, β, and α_1 are present along $\Gamma - R$; a large electron pocket γ is centered at R, followed by another hole pocket, α_2, along $R - M$. The nontrivial nature of the carriers in this band arises from Dirac crossings near E_F along $R - M$ and $R - \Gamma$ lines. These crossings evolve from the triple nodal points under the influence of spin-orbit coupling, as noted in Ref. [9] and can be seen in Fig. 1(d). Figure 1(e) shows the angular dependence of the observed frequencies with solid lines indicating calculated values with E_F at 30 meV (see SM [13] Fig. S3). All frequencies are well accounted for within a full 90° rotation, establishing the three dimensional nature of the FS sheets. This is also evident from the FS plots in Fig. 1(f), where the individual FS sheets are projected into the first Brillouin zone for undoped Pd_3Pb. These results are consistent with those of reference [9]. The η and γ FS sheets are nearly spherical, while α_1 is highly anisotropic with a carrotlike shape, and α_2 is anisotropic and elliptical. The β sheet takes a cubelike shape and encloses η. The observed frequencies and the calculated values are listed in Table S1 of the SM [13]. Overall, theoretical estimates are in reasonably good agreement with experimental observations, except the frequencies $F_{\alpha_{1,2}}$ and F_η are underestimated, similar to an earlier report [11].

From the temperature dependence of the amplitude of the oscillations, we have determined the effective mass of the carriers of the bands $\alpha_{1,2}$, η, and γ (Table S1). For the smaller frequencies, we utilized a combination of data up to 14 T from the PPMS and up to 30 T from NHMFL, and for the larger frequency, F_γ, we used the data taken at NHMFL. As shown in Fig. 2, the fit yields $m*_{\alpha 1} \approx 0.13(2)m_e$, $m*_{\alpha 2} \approx 0.18(4)m_e$, $m*_\eta \approx 0.16(2)m_e$, and $m*_\gamma \approx 0.66(3)m_e$. The experimental values are in excellent agreement with the theoretical estimates. For the β band, the FFT peak amplitude decreases rapidly (see Fig. S1 of the SM [13]), preventing similar LK fits from extracting the effective mass reliably. This indicates a heavier effective mass for this band, consistent with the calculated value of $\approx 1.3m_e$.

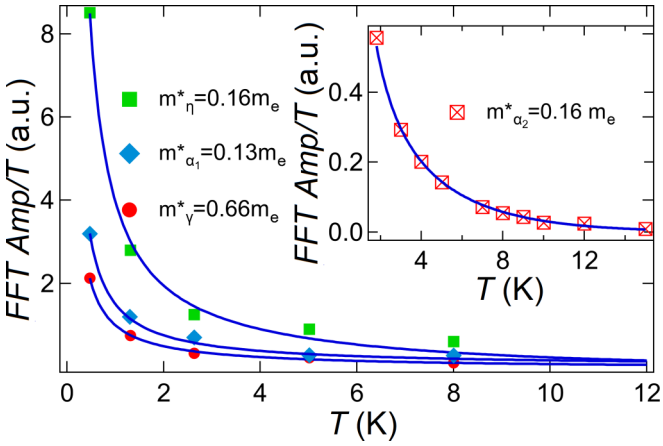

FIG. 2. Band effective mass. LK fit to the temperature dependent amplitude. Inset: LK fit to the 185 T frequency data. Temperature dependence of the FFT peak amplitudes are given in Fig. S1 of the SM [13].

The π-Berry phase accumulated in the cyclotron motion of the quasiparticles is a fundamental property of topological semimetals [20]. The effect of this additional phase factor on quantum oscillations can be studied via the LK formalism developed for a three dimensional (3D) system with arbitrary band dispersion [21–24]:

$$\Delta\rho \propto \left(\frac{B}{2F}\right)^{1/2} R_T R_D R_S \cos\left[2\pi\left\{\frac{F}{B}+\gamma-\delta\right\}\right]. \quad (1)$$

Here, $R_S = \cos(\frac{p\pi g m^*}{2})$, the spin damping factor, p is the harmonic index, and g is the g factor. F is the SdH frequency and the Berry phase, ϕ_B, is related via the phase factor, $|\gamma-\delta|$, where $\gamma = \frac{1}{2} - \frac{\phi_B}{2\pi}$, and δ is related to the dimension of the Fermi pocket with values zero for two dimensional (2D) and $\pm 1/8$ for 3D cases (+ for minimal and − for a maximal cross section of the constant energy surface) [24]. Thus values for $|\gamma-\delta|$, with a nontrivial π-Berry phase, are zero for 2D and 1/8 for 3D Fermi surfaces. If the value of $gm^* \gg 2$, R_S can impart a phase shift in the oscillations, although the Berry phase may be zero. In many d-electron systems, the value of g is large [23], for example, $g \approx 3$ in AuBe [25]. In Pd_3Pb, the absence of a prominent second harmonic in our SdH data [cf. [25]; see Fig. 1(c)] coupled with the small m^* values of the SdH frequencies under consideration suggest that R_S can be neglected safely and that any phase change in our oscillation data is attributable to the effect of a nontrivial Berry phase [23,25].

Using the LK formula, we studied two dominant frequencies, F_{α_1} and F_γ, which arise from the FS sheets that lie along $\Gamma - R$ and $R - M$ and are predicted to be topological [9]. Due to the complex FS, we separated the data ranges where the individual frequencies are dominant. For F_γ, it is evident that this frequency is dominant above 45 T, while for F_{α_1} the relevant field range is below 25 T. The low field data are complicated by other frequencies that contribute to oscillations in varying strengths. From the FFT in low field range (≈9–13 T) at 2 K, we find that, when the field was along 30° and 50° from the crystallographic a axis, F_{α_1} dominates and can be used for LK fit. Figure 3(a) shows a single band LK fit to the oscillation data at 0.5 K and 5 K for the high frequency, F_γ, in the field range 48–58 T with field applied ≈10° from the a axis. At 0.5 K, the fit yields $|\gamma-\delta| = 0.07 \pm 0.03$ indicating a nontrivial topology with a π-Berry phase. From the fit, $F = 1572 \pm 4$ T, consistent with the value we find via FFT, the effective mass, $m^* = 0.65m_e$, similar to the fits in Fig. 2, and the Dingle temperature, $T_D = 35 \pm 3$ K, similar to that reported (42 K) in Ref. [11]. At high fields and low temperatures, the Zeeman splitting between the spin-up and spin-down Fermi surfaces may be noticeable as a pronounced second harmonic in the SdH oscillations, potentially leading to difficulties in attributing a reliable phase. As discussed above, since we do not observe such harmonics, the spin-splitting term can be neglected in the LK fit. However, for completeness, we have used the data at 5 K and performed the LK fit as shown in Fig. 3(a). At higher temperature any residual effect of Zeeman splitting will be reduced by the thermal broadening of the Fermi-Dirac distribution function. The fit yields $|\gamma-\delta| \approx 0.06 \pm 0.02$, in agreement with that found at 0.5 K and confirming the nontrivial Berry phase for this band.

A single band LK fit to the low field data at 2 K for F_{α_1} is shown in Fig. 3(b). At 30°, $|\gamma-\delta| = 0.06 \pm 0.02$, indicating a π-Berry phase. Moreover, F and m^* agree with the values extracted from the FFT and thermal damping fits discussed earlier. The Dingle temperature, $T_D \approx 11 \pm 3$ K, is somewhat smaller than reported in Ref. [11] (25 K). Interestingly, the LK fit to the data at 50° [Fig. 3(b)] yields larger $|\gamma-\delta| = 0.22 \pm 0.06$, indicating an apparent change in the phase with angle. The deviation of the phase factor is also signaled through the shape of the oscillations at this angle, which become sawtooth-like rather than purely sinusoidal.

To explore this behavior, we have investigated the angular dependence of the Berry phase for F_{α_1} between 0° and 90° by rotating the crystal about [0 1 0] with 0° ≈ [1 0 0] and 90° ≈ [0 0 1] and by plotting the oscillation maxima (n) and minima ($n + 1/2$) versus corresponding inverse field values (LL fan diagrams) [26]. For this, we have used the data taken at NHMFL up to 52 T, with LL level $n = 3$, and extracted the F_{α_1} oscillations from the data via a bandpass filtering process [24]. The oscillation minima and maxima were then indexed and plotted as seen in Fig. 3(c) for three different angles (fits for rest of the angles are shown in Fig. S4 of [13]). Here, a linear extrapolation of the data provides the phase factor from the intercept, plotted in Fig. 3(d), while the slope is equal to the frequency of the oscillations and provides a consistency check on the filtering process as well as the estimation of the phase. The horizontal lines in Fig. 3(d) mark the value where the Berry phase for the 3D case is nontrivial (1/8). It is evident that $|\gamma-\delta| \approx 1/8$, except for a sharply peaked region centered at 45°.

Similar angular dependent changes in Berry phase have been reported and attributed to a change in the topological state of the band to a trivial phase. Explanations for this topological phase transition include a quantum phase transition [27,28], a spin zero effect that leads to a new topological phase [29], or an interaction-induced spontaneous mass generation of Dirac fermions [30]. However, in the present case, the

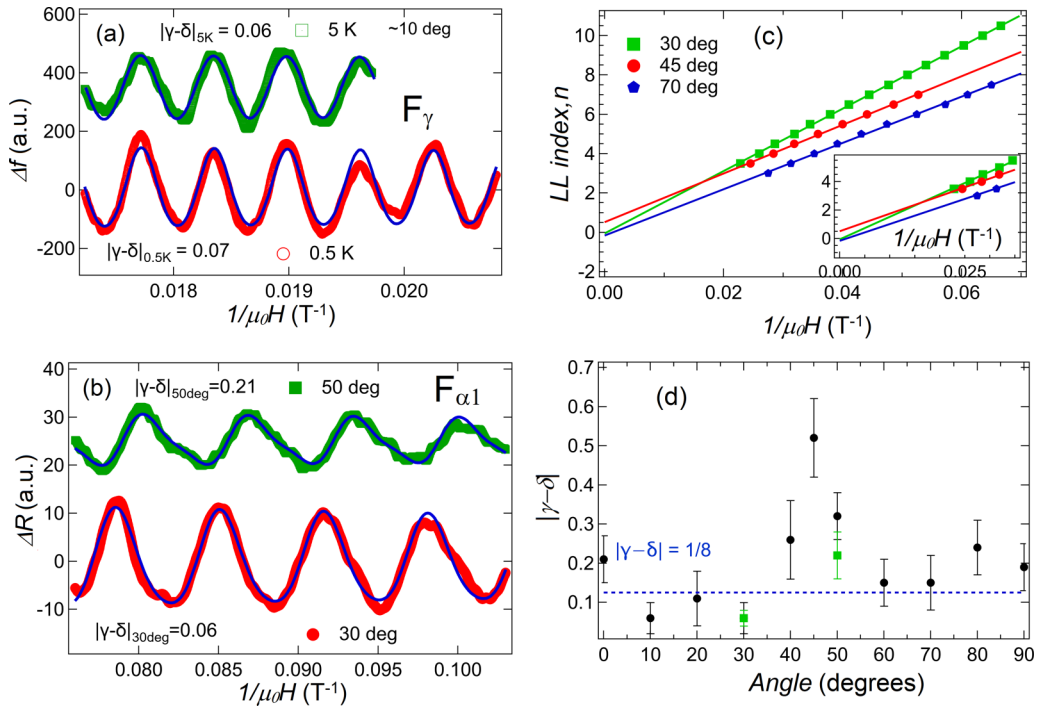

FIG. 3. Berry phase analysis for F_{α_1} and F_γ. (a) A single band LK fit (blue solid line) to the oscillation data for F_γ at 0.5 K (red open circles) and 5 K (olive squares) measured at NHMFL. (b) Single band LK fit (blue solid line) to the oscillation data for F_{α_1} at 30° (red solid circles) and 50° (olive solid squares) and 2 K measured in the PPMS. One higher order harmonic ($2F$) and the fundamental frequency were used for the LK fits. (c) LL-fan diagram for F_{α_1} as described in the text. Inset: expanded view near the origin. (d) Angular dependence of the phase factor for F_{α_1} estimated from the LL-fan plots. At 30° and 50°, values derived from LK fits are plotted and are shown as green solid squares.

maximum value at 45° does not cross the value 5/8 to indicate a phase transition, and a negligible R_S term excludes the possibility of spin-zero effect. The change in phase factor could also arise from the change in the curvature of the Fermi surface, reflected through δ [22,27,30–32]. However, within the precision of the DFT calculations, a change in curvature with respect to the position of the magnetic field for F_{α_1} cannot be resolved.

Based on the nonsinusoidal appearance of the oscillations, we suggest that the apparent phase variation is an artifact due to changes in the relative amplitudes of several series of SdH oscillations that are closely spaced in frequency. This effect may result from the 3D shape of the α_1 FS sheet and its position close to the γ sheet. As the crystal is rotated from the high symmetry direction (i.e., a axis) close to 45°, the different α_1 sheets [see Fig. 1(f)] will possess slightly different extremal orbits, resulting in a smearing of the observed oscillations due to the presence of several similar frequencies, and rendering the phase difficult to extract. Moreover, close to this angle, magnetic breakdown could occur due to the tunneling of carriers between α_1 and γ [23]. As the field grows, this will reduce the fraction of quasiparticles completing orbits about these α_1 sheets, attenuating the corresponding SdH oscillations, while leaving those not subject to breakdown unaffected. Support for this explanation is provided by the unexpectedly large Dingle temperatures found for the oscillations associated with γ (≈35 K) and α_1 (≈11 K) in this angular range. However, the FFT data at 45° (see SM [13] Fig. S5) do not reveal clear evidence of sum or difference frequencies due to the proposed breakdown orbits. It is possible that such oscillations may be weak due to a relatively large effective mass associated with the breakdown orbit.

III. CONCLUSION

In summary, we have studied the Fermi surface topology of the semimetal Pd_3Pb with a combination of low- and high-field measurements and validated the topological nature of this compound predicted by theory. We have experimentally mapped the complete FS, including a hole pocket that had previously been unresolved. Corroborating recent calculations [9], we find evidence of π-Berry phase and hence nontrivial topology for two bands that lie along $\Gamma - R$ and $R - M$ lines. Finally, we point out that the study of the angular variation of the phase factor is important for the systems with complex Fermi surfaces. Incorrect assignment of trivial or nontrivial Berry phases can result from the analysis of the oscillations with field along a single direction.

ACKNOWLEDGMENTS

This research was sponsored by the US Department of Energy, Office of Science, Basic Energy Sciences, Materials Sciences and Engineering Division. P.C. acknowledges support from the US Department of Energy Grant No. DE-SC0014337. A portion of this work was performed at the National High Magnetic Field Laboratory, which is supported by National Science Foundation (NSF) Cooperative Agreements

No. DMR-1157490 and No. 1644779, the State of Florida, and the US Department of Energy (DOE) through the Basic Energy Science Field Work Proposal "Science in 100 T." We thank I. Martin and U. Welp for useful discussions.

[1] B. Yan and S.-C. Zhang, Rep. Prog. Phys. **75**, 096501 (2012).
[2] Y. Ando and L. Fu, Annu. Rev. Condens. Matter Phys. **6**, 361 (2015).
[3] Z. Zhu, G. W. Winkler, Q. S. Wu, J. Li, and A. A. Soluyanov, Phys. Rev. X **6**, 031003 (2016).
[4] B. Bradlyn, J. Cano, Z. Wang, M. Vergniory, C. Felser, R. J. Cava, and B. A. Bernevig, Science **353**, aaf5037 (2016).
[5] Z. Wang, A. Alexandradinata, R. J. Cava, and B. A. Bernevig, Nature (London) **532**, 189 (2016).
[6] S. Mühlbauer, B. Binz, F. Jonietz, C. Pfleiderer, A. Rosch, A. Neubauer, R. Georgii, and P. Böni, Science **323**, 915 (2009).
[7] B. Yan and C. Felser, Annu. Rev. Condens. Matter Phys. **8**, 337 (2017).
[8] M. Leijnse and K. Flensberg, Semicond. Sci. Technol. **27**, 124003 (2012).
[9] K.-H. Ahn, W. E. Pickett, and K.-W. Lee, Phys. Rev. B **98**, 035130 (2018).
[10] N. J. Ghimire, M. A. Khan, A. S. Botana, J. S. Jiang, and J. F. Mitchell, Phys. Rev. Materials **2**, 081201 (2018).
[11] K. Wei, K.-W. Chen, J. N. Neu, Y. Lai, G. L. Chappell, G. S. Nolas, D. E. Graf, Y. Xin, L. Balicas, R. E. Baumbach, and T. Siegrist, Phys. Rev. Materials **3**, 041201 (2019).
[12] J. Singleton, C. Mielke, A. Migliori, G. Boebinger, and A. Lacerda, Physica B: Condens. Matter **346**, 614 (2004).
[13] See Supplemental Material at http://link.aps.org/supplemental/10.1103/PhysRevB.101.245113 for experimental detail, electronic structure calculation,band properties with respect to chemical potential, and LL-fan diagrams, which includes Refs. [11,14–19].
[14] S. Ghannadzadeh, M. Coak, I. Franke, P. Goddard, J. Singleton, and J. L. Manson, Rev. Sci. Instrum. **82**, 113902 (2011).
[15] M. Altarawneh, C. Mielke, and J. Brooks, Rev. Sci. Instrum. **80**, 066104 (2009).
[16] P. C. Ho, J. Singleton, P. A. Goddard, F. F. Balakirev, S. Chikara, T. Yanagisawa, M. B. Maple, D. B. Shrekenhamer, X. Lee, and A. T. Thomas, Phys. Rev. B **94**, 205140 (2016).
[17] P.-C. Ho, J. Singleton, M. Maple, H. Harima, P. Goddard, Z. Henkie, and A. Pietraszko, New J. Phys. **9**, 269 (2007).
[18] G. Kresse and D. Joubert, Phys. Rev. B **59**, 1758 (1999).
[19] J. P. Perdew, K. Burke, and M. Ernzerhof, Phys. Rev. Lett. **77**, 3865 (1996).
[20] A. Burkov, Nat. Mater. **15**, 1145 (2016).
[21] J. Hu, J. Liu, D. Graf, S. Radmanesh, D. Adams, A. Chuang, Y. Wang, I. Chiorescu, J. Wei, L. Spinu *et al.*, Sci. Rep. **6**, 18674 (2016).
[22] H. Murakawa, M. Bahramy, M. Tokunaga, Y. Kohama, C. Bell, Y. Kaneko, N. Nagaosa, H. Hwang, and Y. Tokura, Science **342**, 1490 (2013).
[23] D. Shoenberg, *Magnetic Oscillations in Metals* (Cambridge University Press, Cambridge, UK, 2009).
[24] M. A. Khan, D. E. Graf, I. Vekhter, D. A. Browne, J. F. DiTusa, W. A. Phelan, and D. P. Young, Phys. Rev. B **99**, 020507(R) (2019).
[25] D. J. Rebar, S. M. Birnbaum, J. Singleton, M. Khan, J. C. Ball, P. W. Adams, J. Y. Chan, D. P. Young, D. A. Browne, and J. F. DiTusa, Phys. Rev. B **99**, 094517 (2019).
[26] Y. Ando, J. Phys. Soc. Jpn. **82**, 102001 (2013).
[27] M. N. Ali, L. M. Schoop, C. Garg, J. M. Lippmann, E. Lara, B. Lotsch, and S. S. Parkin, Sci. Adv. **2**, e1601742 (2016).
[28] Z. J. Xiang, D. Zhao, Z. Jin, C. Shang, L. K. Ma, G. J. Ye, B. Lei, T. Wu, Z. C. Xia, and X. H. Chen, Phys. Rev. Lett. **115**, 226401 (2015).
[29] J. Wang, J. Niu, B. Yan, X. Li, R. Bi, Y. Yao, D. Yu, and X. Wu, Proc. Natl. Acad. Sci. USA **115**, 9145 (2018).
[30] Y. Liu, X. Yuan, C. Zhang, Z. Jin, A. Narayan, C. Luo, Z. Chen, L. Yang, J. Zou, X. Wu *et al.*, Nat. Commun. **7**, 12516 (2016).
[31] L. P. He, X. C. Hong, J. K. Dong, J. Pan, Z. Zhang, J. Zhang, and S. Y. Li, Phys. Rev. Lett. **113**, 246402 (2014).
[32] J. Cao, S. Liang, C. Zhang, Y. Liu, J. Huang, Z. Jin, Z.-G. Chen, Z. Wang, Q. Wang, J. Zhao *et al.*, Nat. Commun. **6**, 7779 (2015).